Pure Appl. Chem., Vol. 81, No. 8, pp. 1423–1439, 2009.
doi:10.1351/PAC-CON-08-08-09

Electrochemistry of refractory metals in molten salts: Application for the creation of new and functional materials*

Sergey A. Kuznetsov

Institute of Chemistry, Kola Science Center RAS, Apatity, Murmansk region 184209, Russia

Abstract: The processes of refractory metal complex electroreduction in transition from chloride to chloride–fluoride and oxofluoride melts have been studied. Decrease of the stage number of process complex electroreduction to metal and the possibility of a large number of electrons transferred in a single electrochemical stage on increasing the melt basicity has been established. It was shown that decreasing the stage number of electrode processes can be achieved by the change in anion composition (the first coordination sphere) and, in a number of cases, by the change in the cation composition (the second coordination sphere). With the melt basicity increase, a transition from reversible processes of the complex to metal discharge irreversible ones is observed, as a rule. The knowledge of electrode and chemical reactions accompanying the electroreduction of refractory metals and the study of the processes of alloy formation allow us to obtain novel niobium compounds and functional materials.

Keywords: electrochemistry; refractory metals; molten salts; electroreduction; oxofluoride melts; niobium compounds.

INTRODUCTION

One of the best routes to the economical use of refractory metals is to change, for example, from all-niobium to composite materials. Inexpensive and common metals (e.g., steel, copper, or some of their alloys) serve as substrates for the required mechanical, thermal, or other properties of a device, and niobium coating provides resistance to corrosion and protects the substrate from contact with aggressive environments. Coatings of this kind can also provide an article with desirable electrophysical characteristics (e.g., rectification or superconduction). So, the use of composite material makes the desired objectives possible with minimal consumption of the expensive refractory metal. The electrolysis of molten salts has an advantage over other known methods of plating. It permits pure, plastic, nonporous, and coherent layers of refractory metals to be coated on substrates of complex configuration and large size. There is also an alternative electrolysis application: a refractory metal electrodeposited in thick layers on a bar of low-cost metal replicates the inner surface of the article to be fabricated; subsequent removal of the bar leaves a hollow-shell refractory metal (e.g., for high-frequency superconducting accumulators of energy). Finally, the electrolysis of molten salts is an effective method for recycling re-

*Paper based on a presentation at the 8th Conference on Solid State Chemistry, 6–11 July 2008, Bratislava, Slovakia. Other presentations are published in this issue, pp. 1345–1534.

fractory metals and their alloys. Knowledge of the electrochemistry refractory metals provides data for optimization of electrolytic processes.

SOME ASPECTS OF THE ELECTROCHEMICAL BEHAVIOR OF REFRACTORY METAL COMPLEXES

By varying the anionic and cationic composition of the melt, concentration, and temperature, one is in a position to control the electroreduction of refractory metals [1]. Therefore, it is important to study how these factors affect both the number of steps and the mechanism involved in the electroreduction.

Anionic composition

The number of steps and the mechanism involved in the electroreduction of complexes are affected most strongly, by the anionic composition of the melt, as it determines the composition of the first coordination sphere. The relevant data on the effect of the anionic composition of the melt on the mechanism involved in the electroreduction of refractory metal complexes in a NaCl–KCl melt are listed in Table 1.

Table 1 Effect of the anionic composition of the melt on the steps and mechanism involved in the electroreduction of refractory metal complexes in the NaCl–KCl melt.

Element	Mechanism of electroreduction in melts		
	Chloride	Chloride–fluoride	Oxofluoride
Hf [1–4]	I Hf(IV) + $2e^-$ → Hf(II) (R); at $\nu \leq 0.66$ V/s complicated by DPP reaction II Hf(II) + $2e^-$ → Hf (IR)	I Hf(IV) + $4e^-$ → Hf (IR)	
Nb [13–15,19]	I Nb(V) + e^-→ Nb(IV) (R) II Nb(IV) + $4e^-$ → Nb (R)	I Nb(V) + e^- → Nb(IV) (R) II Nb(IV) + $4e^-$ → Nb (IR)	I Nb(V) + $5e^-$ → Nb(Q); at $\nu \leq 2.0$ V/s complicated by preceding chemical reaction
Cr [1,20]	I Cr(III) + e^- → Cr(II) (R) II Cr(II) + $2e^-$ → Cr (R)	I Cr(III) + e^- → Cr(II) (R) II Cr(II) + $2e^-$ → Cr (IR)	I Cr(VI) + $3e^-$ → Cr(III) end product Cr_2O_3
Re [8,11]	I Re(IV) + e^- → Re(III) (R) II Re(III) + $3e^-$ → Re (R)	I Re(IV) + e^- → Re(III) (R) II Re(III) + $3e^-$ → Re (IR)	I Re(VII) + $7e^-$ → Re (IR)
Ir [1,10]	I Ir(IV) + e^- → Ir(III) (R) II Ir(III) + $3e^-$ → Ir (R)	I Ir(IV) + $4e^-$ → Ir (IR)	I Ir(VI) + $6e^-$ → Ir (IR)

Note: (R), reversible process; (IR), irreversible process controlled by charge transfer rate; (Q) quasi-reversible process.

The influence exerted by the anionic composition of the melt depends on the element, but a common feature is that an increase in the basicity of the melt reduces the number of discharge steps and causes the discharge of complexes to the metal to change from a reversible to an irreversible process.

Cationic composition

The effect of the cationic composition of the melt on the number of steps involved in electroreduction for hafnium has been observed on changing from NaCl–KCl to CsCl. When about 70 mol % cesium chloride was added to the NaCl–KCl–$HfCl_4$ melt, the two-step mechanism of electroreduction with a two-electron discharge at each step gave way to a one-step mechanism with a four-electron discharge

of hafnium complexes to the metal [2,3]. This change in the electroreduction mechanism is traceable to the replacement of potassium and sodium cations by cesium in the second coordination sphere of the $HfCl_6^{2-}$ complexes. One-step irreversible discharge of HfF_6^{2-} complexes has also been reported in an equimolar NaCl–KCl mixture [4,5]. Drawing upon Lux's view on the acidic–basic properties of ionic melts, one may conclude that the increase in the basicity of the melt, due to a change in the anionic or cationic composition, is responsible for the transition from the two-step mechanism with a two-electron discharge at each step in the NaCl–KCl–$HfCl_4$ melt [6,7] to the irreversible one-step mechanism in the NaCl–KCl–K_2HfF_6 [4] and CsCl–$HfCl_4$ [2,3].

A change in the second coordination sphere can give rise to additional waves on voltammetric curves. It has been established that the NaCl melt contains solely Re(III) complexes, which are characterized by a single wave corresponding to $Re(III) + 3e^- \rightarrow Re$ [8]. When 60 mol % potassium chloride or 70 mol % cesium chloride is added to NaCl, the sodium cations are displaced from the second coordination sphere by potassium or cesium. In the melt, Re(IV) complexes are formed. They are characterized by the electroreduction wave $Re(IV) + e^- \rightarrow Re(III)$. A higher concentration of CsCl is required because cesium has a lower ionic potential than potassium. The second coordination sphere likewise affects the electroreduction mechanism: the process $Re(III) + 3e^- \rightarrow Re$ is reversible in sodium and potassium chlorides, but irreversible in the CsCl melt [8].

Temperature

The temperature effect on the mechanism of electroreduction niobium complexes has been observed in the LiCl–KCl–$NbCl_5$ melt [9]. At a temperature below 903–923 K, the electroreduction of niobium proceeds in a three-step mechanism:

$$\text{I} \qquad Nb(V) + e^- \rightarrow Nb(IV) \text{ (reversible)} \tag{1}$$

$$\text{II} \qquad Nb(IV) + 2e^- \rightarrow Nb(II) \text{ (irreversible)} \tag{2}$$

$$\text{III} \qquad Nb(II) + 2e^- \rightarrow Nb \text{ (reversible)} \tag{3}$$

It should be added that the second step of electroreduction is complicated by the formation of insoluble cluster compounds owing to the reaction of Nb(IV) and Nb(II) complexes. At the second step, $NbCl_{2.33}$ cluster compound and a large assortment of nonstoichiometric compounds in the composition range $NbCl_{2.67}$–$NbCl_{3.13}$ have been obtained by potentiostatic electrolysis. The electrolysis at more negative potentials leads to an increased amount of niobium in the cathodic deposit. At the third step, the Nb(II) complexes still not reacted with Nb(IV), or reduced from cluster compounds, are discharged to the metal. At temperatures above 923 K, the second and third waves merge into a single four-electron wave, and the formation of cluster compounds of the $NbCl_x$, type becomes thermodynamically unfeasible. The voltammograms display only two reduction waves:

$$Nb(V) + e^- \rightarrow Nb(IV) \text{ (reversible)} \tag{4}$$

$$Nb(IV) + 4e^- \rightarrow Nb \text{ (reversible)} \tag{5}$$

At a temperature higher than 923 K, the deposition of niobium is not complicated by the formation of subchloride impurities.

According to [10], when in the cathodic reduction of iridium, $Ir(III) + 3e^- \rightarrow Ir$, in a NaCl–KCl–CsCl eutectic melt the temperature is raised to 873 K, the process changes from irreversible to reversible, and this in turn causes the structure of the deposits to change from coherent to dendritic.

Concentration

With an increasing of the metal-containing component concentration, one finds it somewhat difficult to analyze voltammetric curves and to cancel out the ohmic component in obtaining voltammograms.

During the electrodeposition of rhenium coatings from the NaCl–KCl melt at a rhenium concentration of 5.0 wt % and a current density of higher than 0.05–0.07 A cm^{-2}, rhenium metal powder and the salt are deposited at the cathode. Voltammograms for the NaCl–KCl electrolyte containing 5.0 wt % of rhenium show an extra wave at more negative potentials. Potentiostatic electrolysis at the potentials of the first wave results in the formation of a rhenium coating. Electrolysis at the potentials of the second wave yields rhenium powder or rhenium sponge. In addition to the metal, a dark green salt was discovered on the cathode. X-ray diffraction (XRD) analysis and chemical analyses identify this salt as $K_2Re_2Cl_8$ whose formation can be explained only by the participation in the second discharge process of the polynuclear rhenium complexes that are likely to appear in melts of high rhenium concentration [11]. Strubinger et al. [12] reported the following polynuclear complexes of rhenium: $[Re_2Cl_8]^{2-}$, $[Re_2Cl_8]^{3-}$, $[Re_3Cl_{12}]^{3-}$, and $[Re_3Cl_{11}]^{3-}$. The formation of $K_2Re_2Cl_8$ at the cathode indicates that trinuclear rhenium complexes must be participating in the discharge process along with the formation of binuclear complexes. The reduction of trinuclear rhenium complexes may be assumed to proceed according to

$$4[Re_3Cl_{12}]^{3-} + 2K^+ + 5e^- \rightarrow K_2Re_2Cl_8 + 5[Re_2Cl_8]^{3-} \quad (6)$$

Connection between the number of electroreduction stages and thermodynamic stability of complexes

The number of electroreduction steps is connected with the thermodynamic stability of refractory metal complexes of various oxidation states at given acid–base properties of the melt. By voltammetry in the NaCl–KCl melts at a ratio of $[F^-]/[Hf^{4+}] < 5$, three cathodic peaks are associated with the reduction of the Hf(IV) species in the chloride–fluoride Hf(IV) complexes to Hf(II), the discharge of Hf(II) to the metal and the electroreduction of Hf(IV) fluoride complexes to hafnium in one four-electron step [13]. The formation of Hf(IV) fluoride complexes is due to generation of fluoride anions in the vicinity of the cathode as the result of the Hf(II) chloride–fluoride complexes discharge and following ligand exchange reaction. At a ratio of $[F^-]/[Hf^{4+}] \geq 5$, only one cathodic four-electron wave is observed. Thus, an increase in the number of fluoride anions in hafnium ligand shell results in Hf(IV) stabilization and a change in the discharge mechanism [13].

The conditions for stabilization of the highest oxidation states of refractory metals in NaCl–KCl melts have been determined in [14]. The changes of the most stable oxidation states of various d-elements in NaCl–KCl molten salt from purely chloride to oxochloride, chloride–fluoride, and oxofluoride complexes are given in Table 2.

Table 2 Oxidation states of refractory metals in NaCl–KCl molten salt.

	Composition of complexes					Composition of complexes					Composition of complexes			
3d*	Cl	O–Cl	Cl–F	O–F	4d*	Cl	O–Cl	Cl–F	O–F	5d*	Cl	O–Cl	Cl–F	O–F
Ti	II–IV	III, IV	III, IV	IV	Zr	II, IV	IV	IV	IV	Hf	II, IV	IV	IV	IV
Cr	II, III	III, V, VI	II, III	VI	Nb	IV, V	V	IV, V	V	Ta	IV, V	V	V	V
										Re	III, IV	V–VII	III, IV	VI, VII
										Ir	III, IV	V, VI	IV	VI

*Elements: Cl, chloride; O–Cl, oxochloride; Cl–F, chloride–fluoride; O–F, oxofluoride.

The stabilization of higher oxidation states is often observed when passing from pure chloride, oxochloride, and chloride–fluoride to oxofluoride melt. This trend revealed for the alkali-halide melts containing d-elements is supported by numerous data on stabilization of the highest oxidation states in solutions and in solid phase. These data show that anionic ligands as F^- and O^{2-} are preferable for stabilizing the highest oxidation states. The highest valences obtained in chloride–fluoride or oxofluoride melts are often the same. But oxofluoride melts are preferable for stabilizing the highest oxidation states of chromium, niobium, rhenium, and iridium. Obviously, in these melts the effect of fluorine electronegativity and the stabilizing effect of electron delocalization typical for oxygen are acting synergistically. For instance, the highest oxidation state +7 was obtained for rhenium in the oxofluoride melt [8]. By addition of oxygen anions to NaCl–NaF melts at various ratios of $[O^{2-}]/[Re^{4+}]$, the Re(VI) and Re(VII) complexes can be stabilized.

Formation of complexes of different composition in the vicinity of the electrode differing from the complexes in the bulk of the melt

Voltammetric curves for the NaCl–KCl–NaF (5 wt %)-K_3NbOF_6 melt at different polarization rates allowed us to discover that, in the voltammograms recorded at $\nu \leq 0.1$ V s^{-1}, a second peak appears at more negative potentials [13–15]. As the polarization rate was decreased, the ratios between the heights of the first and second peak change in favor of the latter peak. Such behavior observed in the presence of solely monoxofluoride complexes in the melt can be explained by the generation of free oxygen anions by discharge of $NbOF_6^{3-}$ in the vicinity of the electrode and by occurrence of the exchange reaction

$$NbOF_6^{3-} + O^{2-} \leftrightarrow NbO_2F_4^{3-} + 2F^- \quad (7)$$

Dioxofluoride complexes that are formed by reaction 7 discharge at more negative potentials than monoxofluoride ones [13]. The appearance of the second peak and its height are controlled by the ratio between the rates of polarization and exchange reaction 7.

Multi-electron transfer in narrow interval potentials at heteronuclear complexes discharge with formation of compounds

The formation of heteronuclear complexes is important not only for high-temperature coordination chemistry but also for electrochemistry and electrolytic alloys. Indeed, during the discharge of heteronuclear complexes, conditions are created for the direct formation of an alloy. The refractory boride synthesis by joint deposition of components from molten salts becomes energetically more favorable if the components are complexed in heteronuclear complex ions, consisting of boron–refractory metal bonds [16]. The suggestion of the existence of heteronuclear complexes originates from the results of electrochemical experiments rather than from straightforward structural studies. At the present time, spectroscopic data on heteronuclear complexes formation were obtained for low-temperature melts on the $AlCl_3$ base [17]. The following experimental facts based on voltammograms can be explained by the existence of heteronuclear complexes:

- Although the individual components (B and Me) are deposited in irreversible electrochemical reaction, the electrochemical synthesis of some borides takes place as a reversible reaction. For example, for the NaCl–KCl–NaF–KBF_4–K_2TiF_6 system, the synthesis wave of TiB_2 is reversible and is limited by diffusion of ions in the melt [18], although the deposition of boron in the NaCl–KCl–NaF–KBF_4, and that of titanium in the NaCl–KCl–NaF–K_2TiF_6 system take place irreversibly and are limited by the charge transfer;
- In some cases, an initial chemical reaction takes place prior to the charge transfer during electrochemical synthesis of borides; these preceding reactions can be interpreted as formation or dis-

sociation of heteronuclear complexes. For example, in the NaCl–KCl–NaF–KBF_4–K_2HfF_6 [19] and NaCl–KCl–NaF–KBF_4–K_2TaF_7 [20] systems, the existence of the initial chemical reaction prior to the charge transfer was found based on electrochemical criteria [21];

- Diffusion coefficients of electrochemically active species during the electrochemical synthesis of borides (calculated from voltammograms) appear to be much smaller, as compared with those obtained in melts consisting only of boron ions, or ions of the metallic component of the boride. For example, the diffusion coefficients of electrochemically active species (T = 973 K) used for synthesis of TiB_2, ZrB_2, and HfB_2 equal 8.9×10^{-6}, 9.9×10^{-6}, 4.0×10^{-6} $cm^2\ s^{-1}$ correspondingly, being 2–3 times lower than the diffusion coefficients of "pure" Ti, Zr, Hf, or B-complexes [22]. This is obviously due to the larger size of the electrochemically active species during synthesis of borides compared to those during deposition of metals or boron; indicating the formation of heteronuclear species.

One of the most challenging phenomena in boride electrochemical synthesis is the formation of periodically layered structure of borides, as in the case of tantalum borides [23]. The coating with a total thickness of 30–50 μm was obtained using constant current density and consisting of numerous sublayers each with thickness less than 1 μm. The formation of such a multi-layered structure was explained by concentration fluctuation near the cathode surface, leading to the appearance of the ever-changing situation of over- and under-saturation of heteronuclear complexes [23].

In the NaCl–KCl melt containing chromium and aluminum chlorides, the formation of heteronuclear complexes was determined, which during discharge formed chromium–aluminum alloy [24]. So in this case, it is possible to obtain the alloy of components with significantly different values of standard potentials. It was shown [25] that in the $AlCl_3$–NaCl (2:1) electrolyte containing Ti(II) complexes at a certain titanium concentration, the $TiAl_3$ intermetallic compound was deposited on the cathode in a wide range of cathodic current density. The authors [25] explained this fact by the $[Ti(AlCl_4)_3]^-$ electroactive-species formation proved by spectroscopy data [17]. In some studies, correlation between the composition of heteronuclear complexes and the composition alloy was found [26].

A multi-electron transfer is also very challenging for general electrochemical kinetics in one stage. During electrochemical synthesis of refractory borides, 10 or even 11 electrons are transferred in one step in the very narrow potential interval. According to classical electrochemical kinetics, multi-electron electrochemical reactions are interpreted as the consecutive sequence of 1-electron transfer. In the case of electrochemical synthesis, even the application of modern electrochemical technique does not allow the division of the 10-electron process into 10 steps of one-electron transfer. Modern quantum-chemical calculations proved the energetic possibility of one-step multi-electron processes against the multi-step one-electron processes in high-temperature molten salts [27].

CREATION OF NEW MATERIALS

In recent years, the behavior of oxygen, especially of oxygen-containing niobium species, in electrochemical processes has drawn the attention of many researchers [28–34]. This fact is apparent: oxygen is one of the most harmful impurities in niobium and adversely affects the mechanical and electrophysical properties of all refractory metals. On the plus side, a series of previously unknown niobium compounds became possible in melts containing niobium oxygen-containing complexes.

Gradual changes are observed in the phase composition of the products, as is evident from the schematic drawing (Fig. 1). The deposits of several primary cycles of electrolysis represent solid solutions of oxygen in niobium, with the successively growing distortion of body-centered lattice symmetry. Further oxidation of the melt produces niobium monoxide in the cathode products. In the products of electrolysis in CsCl-containing melts, phases still more rich in oxygen are present. There are two niobium compounds which were first identified [35]: NbO' and Nb_4O_5. NbO' is a niobium oxide with a disordered distribution of vacancies in the NaCl-type structure, in both in Nb and O positions. Its spe-

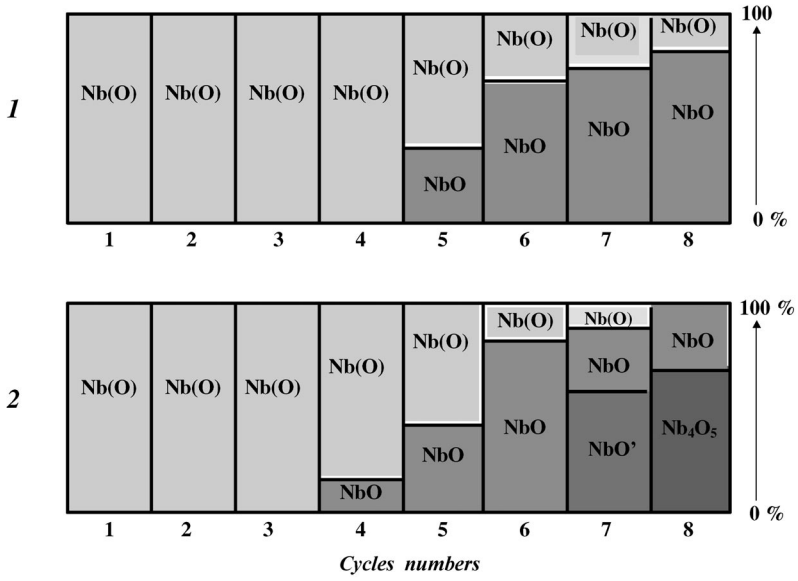

Fig. 1 Gradual changes in phase composition (relative proportions of the phases) of cathode deposits from successive cycles of galvanostatic electrolysis in (*1*) RbCl–K_2NbF_7 and (*2*) CsCl–K_2NbF_7 melts with NbO anode; 0.05 mole K_2NbF_7; 1023 K, I_c = 0.2 A cm^{-2}.

cific feature is that, having the same structural type as that in ordinary NbO, NbO' can contain far more oxygen (up to O/Nb = 1.7), while the range of homogenity of NbO is very narrow (O/Nb = 0.97–1.03). Nb_4O_5 is a novel equilibrium phase in the O–Nb binary system. Due to through channels where Nb–Nb metallic bonds are realized, Nb_4O_5 differs from all niobium compounds earlier known.

Substitution of the rubidium and cesium chlorides by their fluorides as solvents for niobium species results in a principal change in cathodic process in the presence of oxygen in the melt. With these solvents, sufficiently pure niobium metal can be produced at least up to the molar ratio O:Nb = 1, in the melt. The oxygen content in electrolytic niobium was on level of several tenth fractions of 1 % when CsF solvent was used, and several hundredth fractions of 1 % only in the case of RbF solvent.

Thus, we have considered the cathodic behavior of oxygen in the melts, which initially contained oxygen-free niobium complex anions NbF_7^{2-} and gradually obtained more and more niobium monooxofluoride anions, evidently $NbOF_5^{2-}$ or $NbOF_6^{3-}$ [34], generated by NbO anode dissolution. The final point of such monitoring should be the situation when all niobium in the melt is represented by these ions, with no initial niobium fluoride anions. Nevertheless, no visible changes are seen until the end of the monitoring in terms of the electrochemical behavior of oxygen.

In connection with aforesaid, to activate the electrochemical behavior of oxygen, the conditions of electrolysis were made more severe in the next series of electrolysis cycles. All niobium was introduced into the starting electrolyte by using K_2NbOF_5 instead of K_2NbF_7. Thus, during monitoring, the melts passed gradually from the region of existence of monooxofluoride anions to the region of simultaneous existence of mono- and dioxofluoride anions, in which molar ratio O:Nb approached 2.

The results are shown in the schemes of Fig. 2. Here, findings of the present work appear together with earlier results concerning the melts, where the eutectic mixture of NaF and LiF was used as solvent for K_2NbOF_5. As is evident from the schemes, only in this case (**4**), are niobium monoxides formed as cathode products for all cycles of electrolysis from the very first. For all other solvents, the cathode products of the first cycles are solid solutions of oxygen in niobium, or even pure niobium metal. The reason for this difference is an inversion of potentials for the discharge of fluoride and oxofluoride niobium complexes in going from LiF or NaF solvents for niobium species to fluorides with

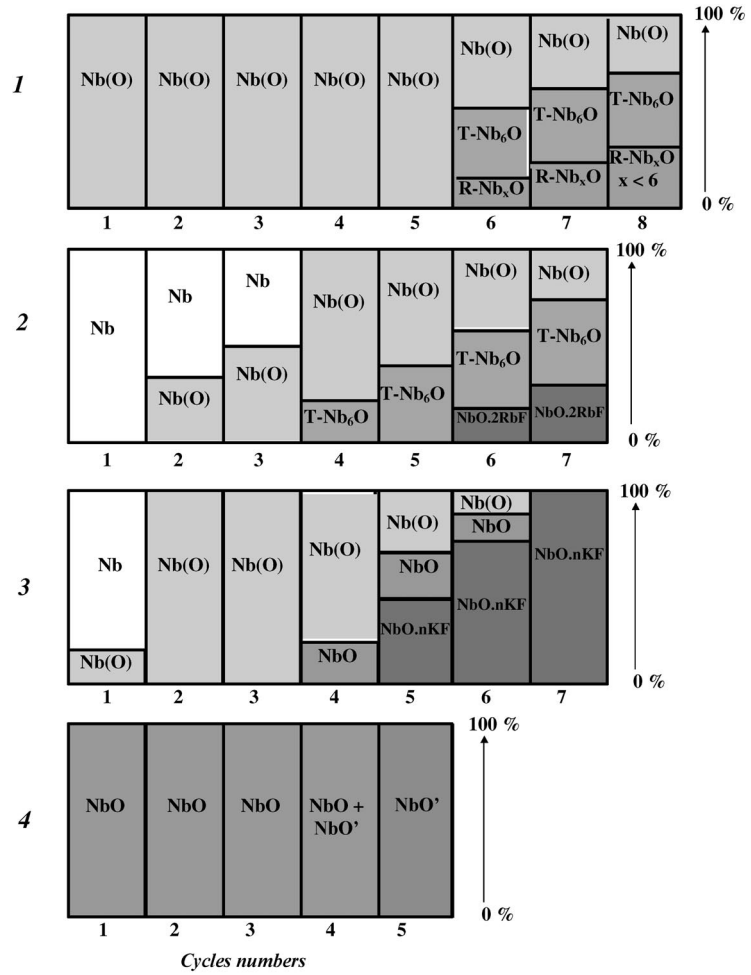

Fig. 2 The gradual change in phase composition (relative proportions of the phases) of cathode deposits from successive cycles of galvanostatic electrolysis in K_2NbOF_5 (*1*) CsF–K_2NbOF_5, (*2*) RbF–K_2NbOF_5, (*3*) KF–K_2NbOF_5, and (*4*) NaF– LiF–K_2NbOF_5 melts with a NbO anode; 0.05 mole K_2NbOF_5; 1023 K; I_c = 0.2 A cm^{2-}. The R- and T-notations correspond to rhombohedral and tetragonal structures, respectively.

bigger cations (KF, RbF, or CsF): the discharge of the oxofluoride complexes becomes more negative than the discharge required for the oxygen-free anions [36].

Toward the end of monitoring, when the melt contains a sufficient amount of dioxofloride complexes, novel phases are deposited at cathode during electrolysis besides solid solutions of oxygen in niobium Nb(O), tetragonal niobium suboxide Nb_6O and NbO. Here there is a previously unknown rhombohedral niobium suboxide Nb_xO (where $x < 6$) in the case of the CsF solvent, and compounds containing niobium of low oxidation state, oxygen, fluorine and potassium or rubidium in the case of KF or RbF solvents, respectively.

We succeeded in finding out, by single-crystal diffraction data, that these compounds have a composite (schistose) structure. The structure of rubidium-containing composite phase may be represented as a combination of two parent structure fragments or two layer blocks conditionally named by us "NbO" and "RbF" [36].

A compound of similar structure type—"NbO"·n "KF"—has been obtained by using KF as solvent, but no phases of this type were obtained working with melts containing LiF, NaF, or CsF. This in-

teresting feature is apparently explained by the fact that the cell parameter *a* of the "MeF" fragment is near the corresponding parameter of the "NbO" fragment *a* = 4.21 Å only when Me = K or Rb. For Na and Li, this cell parameter is too small, and for Cs it is too great [36]. In both cases, there is no matching in corresponding dimensions to build a stable composite structure

It is significant that these novel composite compounds belong to the same structure type as cuprates—widely known high-temperature superconductors.

CREATION OF FUNCTIONAL MATERIALS

Nowadays, coatings are produced mostly by chemical vapor deposition (CVD), PVD methods, plasma and detonation spraying. In a monograph [37], various ways of deposition of the protective coatings are accessed on the basis of the following criteria: principal possibility of production and control; achieving adequate quality; technological and cost parameters. Proceeding from these criteria, one of the most effective methods is plating from molten salts. Molten salts provide the production of coatings by precise surface alloying, electrodeposition, and electrochemical synthesis, and by employing reactions of currentless transfer and disproportionation.

Precise surface alloying of niobium by hafnium

Alloy formation during electrodeposition of hafnium on a niobium cathode from a molten equimolar mixture of NaCl and KCl containing 10 wt % K_2HfF_6 was studied at 1023 K. The investigation was carried out by a chronopotentiometry method. The electrolysis of the melt, which was placed in a container made from type SU-2000 glassy carbon, was carried out with the aid of a P-5848 potentiostat in an electrochemical cell [38]. The recording of the potential of the niobium cathode (a rod with a diameter of 2 mm, which was obtained from an ingot by electron-beam melting) relative to a hafnium reference electrode (a 5 cm^2 plate) was carried out by a KSP-4 potentiometer and a V7-21 digital voltmeter. The potential scan rate for steady-state voltammograms was 5×10^{-3} V s^{-1}, and experiments were carried out at 973–1123 K.

On the charging curves (the cathodic chronopotentiograms) in potential-time coordinates (Fig. 3), which allow for studying the ohmic component, there are four sections with different types of variation of the potential, in agreement with the niobium–hafnium equilibrium diagram [39]. The formation of hafnium in niobium takes place in a β-solid solution between 0 to τ_1. The concentration of hafnium in

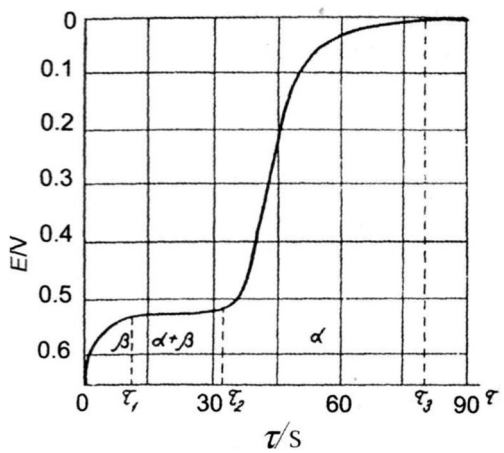

Fig. 3 Dependence of the potential (*E*, V) formed during electrodeposition of hafnium on the niobium cathode on the electrolysis time (τ, s); cathodic current density 8.3×10^{-3} A cm^{-2}, temperature, 1023 K.

it increases. The formation of an (α + β)-solid solution takes place on the section from τ_1 to τ_2. After the limiting concentration of hafnium in the α-solid solution is achieved (at τ_3), a phase of hafnium forms, and pure hafnium grows.

The absence of a potential dependence on the composition (the electrolysis time) is observed in the two-phase (α + β)-region owing to the constant activity of hafnium within the two-phase region. An abrupt variation of the potential is discovered within the α-phase, i.e., the activity of hafnium in the α-phase is very dependent on the concentration.

Charging curves were recorded during the deposition of hafnium on niobium at current densities from 4×10^{-4} to 5×10^{-2} A cm^{-2}. Plots of the dependence of the limiting concentration of hafnium in β-, (α + β)-, and α-phases (Fig. 4) were obtained on the basis of these curves. The curves obtained made it possible to establish the variation of the phase composition during the electrodeposition of hafnium on niobium and to determine the time intervals for the formation and growth of the phases on the surface of the cathode at different current densities and temperature of 1023 K.

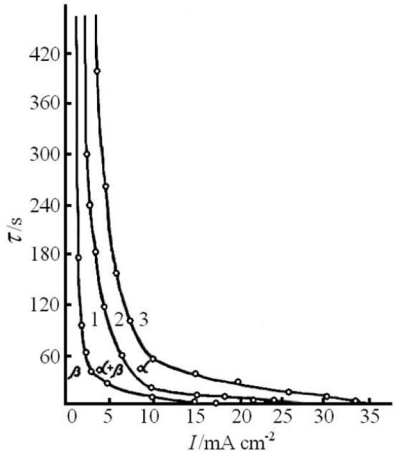

Fig. 4 Time interval for the phases formation and growth on the niobium cathode surface (τ, s) at different current densities (I, A cm^{-2}). Atomic fraction of Hf on section: 1: C = 5.9 at %, β-solid solution section; 2: C = 95.9 at %, (α + β)-solid solution section; section 3: C = 100 at %, α-solid solution.

It follows from Fig. 4 that in order to obtain a β-solid solution of hafnium in niobium, the electrolysis process must be carried out at a very low current density, i.e., at a current density not exceeding 1×10^{-3} to 2×10^{-3} A cm^{-2}. Hafnium coatings can be obtained on a niobium substrate with intermediate layers of solid solutions of hafnium in niobium at current densities ranging from 4×10^{-3} to 3×10^{-2} A cm^{-2}. The formation of intermediate layers of solid solutions guarantees good adherence of the hafnium coating to the niobium substrate. The use of a current density higher than 3×10^{-2} A cm^{-2} results in the formation of metallic hafnium only on the surface of the niobium substrate.

On the basis of chronopotentiometric curves obtained at different cathodic current densities, the parameters of the solid-state interdiffusion coefficients for the couple Hf–Nb can be determined. According to [40], the coefficient $\tilde{D}$ of interdiffusion in the case of solid solution formation of deposited metal with material of the cathode can be calculated by the type Sand equation

$$N = 2V_a i\tau^{1/2}/nF\,\pi^{1/2}\,\tilde{D}^{1/2} \tag{8}$$

where N is the atomic fraction of Hf, V_a the molar volume of alloy (cm^3 mol^{-1}), I the cathodic current density (A cm^{-2}), τ the transition time of the solid solution formation, n the number of electrons involved in the reaction, F the Faraday constant 96 487 C mol^{-1}, $\tilde{D}$ the interdiffusion coefficient for the couple Hf–Nb (cm^2 s^{-1}).

Equation 8 is valid under the following conditions: the molar volume of the alloy is invariable; the interdiffusion coefficient is constant and does not depend on the concentration. Using eq. 8, it was found that the interdiffusion coefficients for the couple Hf–Nb at 1023 K in β- and (α + β)-phases are $(2.2 \pm 0.6) \times 10^{-10}$ and $(3.2 \pm 0.4) \times 10^{-12}$ cm^2 s^{-1}, respectively.

Thus, $\tilde{D}$ in (α + β)-phase is by two orders of magnitude smaller than in the β-phase. These confirm the correlation between interdiffusion coefficients in phases of different compositions and their heat resistance. It is known that the heat resistance of Nb–Hf alloys corresponding to compositions of (α + β)-solid solutions are higher than those of the β-phase [41].

Parameters for the formation of the (α + β)-phase of Nb–Hf alloys were used for the modification of niobium coatings on graphite substrates. The disadvantage of the above-described method is the insignificant thickness of the Nb–Hf alloy that leads to a certain limitation of the composite working. Thicker coatings can be obtained by high-temperature electrochemical synthesis from molten salts containing compounds of niobium and hafnium.

Electrochemical synthesis of Nb–Hf coatings

The electrolyte NaCl–KCl–K_2NbF_7 (1 wt %)–K_2HfF_6 (10 wt %)–NaF (5 wt %) and niobium anode were used for electrochemical synthesis. In contact with niobium anode, due to the interaction

$$4\ \mathrm{Nb(V)} + \mathrm{Nb} \leftrightarrow 5\ \mathrm{Nb(IV)} \tag{9}$$

complexes of Nb(IV) exist only in the melt.

Electrodeposition of Nb–Hf coatings occurs in the "kinetic regime" [16,42] due to significant difference of formal standard potentials $E^*_{\mathrm{Nb(IV)/Nb}} - E^*_{\mathrm{Hf(IV)/Hf}}$. The kinetic regime appears if the deposition potentials of components on inert cathodes are too far from each other. A scheme of electrodeposition of Nb–Hf alloys is presented in Fig. 5. As can be seen from Fig. 5, the deposition of niobium at current density (I) less than limiting current density of discharge niobium complexes $I_{\mathrm{lim}}^{\mathrm{Nb}}$ at the graphite cathode, is observed. At $I > I_{\mathrm{lim}}^{\mathrm{Nb}}$, electrodeposition of niobium and hafnium takes place simultaneously. With increasing current density, the growth of hafnium concentration in the alloy was observed.

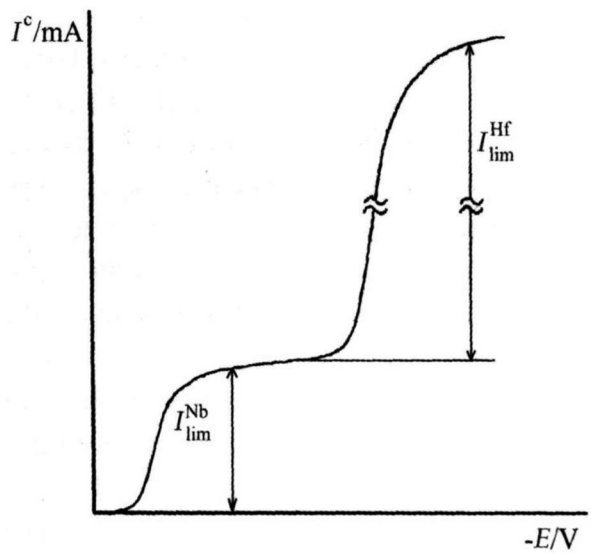

Fig. 5 Scheme of electrodeposition of Nb–Hf alloys from NaCl–KCl–K_2NbF_7 (1 wt %)–K_2HfF_6 (10 wt %)–NaF (5 wt %) electrolyte in contact with the niobium anode.

The steady-state voltammetry method was used for the determination of the limiting current density of discharge Nb(IV) complexes in NaCl–KCl–K_2NbF_7 (1 wt %)–K_2HfF_6 (10 wt %)–NaF (5 wt %) electrolyte, which was in equilibrium with metallic niobium. For steady-state voltammetry at constant temperature, the next equation is valid

$$I_{\text{lim}}^{\text{Nb}} = kC_{\text{Nb(IV)}} \tag{10}$$

where k is diffusion constant for limiting current density (A cm^{-2} wt %$^{-1}$), $C_{\text{Nb(IV)}}$ the concentration of Nb(IV) complexes (1.25 wt % in our case).

The limiting current density is satisfactorily fitted by the empirical dependence

$$I_{\text{lim}}^{\text{Nb}} = 15.2 \times 10^{-2342/T} C_{\text{Nb(IV)}} \tag{11}$$

Equation 11 allows us to calculate the limiting current density for the above-mentioned electrolyte at different temperatures.

In the case of the "kinetic regime", the ratio of the niobium and hafnium concentrations in the alloy is described by the following equation [43]:

$$C_{\text{Nb}}/C_{\text{Hf}} = (I_{\text{lim}}^{\text{Nb}} n_{\text{Hf}})/[(I - I_{\text{lim}}^{\text{Nb}}) n_{\text{Nb}}] \tag{12}$$

where n_{Hf} and $n_{\text{Nb}} = 4$, C_{Nb} and C_{Hf} are the concentrations of niobium and hafnium (wt %) in the alloy.

So, for the "kinetic regime", the synthesis of Nb–Hf alloys takes place if the applied current density is higher than the limiting current density of electropositive component (Nb). It was shown that Nb–Hf coatings with a planar growing front can be obtained if the concentration of the more electropositive component is low and therefore the limiting current density ($I_{\text{lim}}^{\text{Nb}}$) is low too. Optimal cathodic current densities for the electrodeposition of Nb–Hf coatings with the thickness 20–30 μm were determined. The scanning electron microscopy (SEM) image of Nb–Hf coating obtained from an NaCl–KCl–K_2NbF_7 (1 wt %)–K_2HfF_6 (10 wt %)–NaF (5 wt %) electrolyte with a niobium anode at a cathodic current density 0.12 A cm^{-2} and the temperature 1023 K is presented in Fig. 6. Electron probe microanalysis (EPMA) of some Nb–Hf alloys obtained at different cathodic current densities shows a good agreement between calculated (eq. 12) and experimental data. The scanning images of the Nb–Hf alloys with 78.1 and 33.8 wt % Nb in characterizing rays Nb–L_α are shown in Fig. 7.

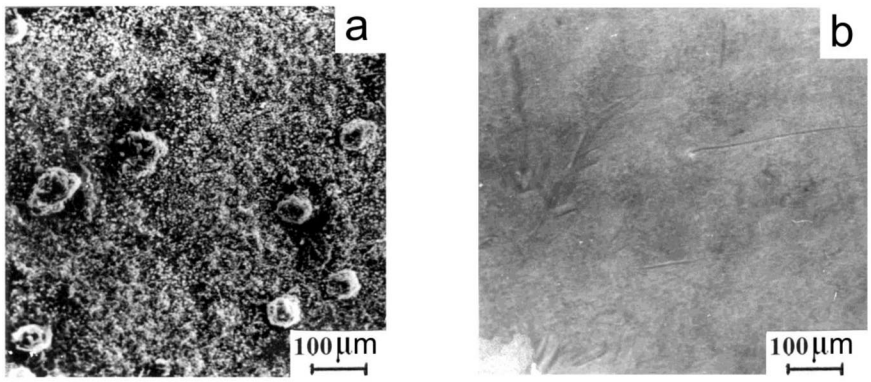

Fig. 6 SEM image of Nb–Hf coating obtained from NaCl–KCl–K_2NbF_7 (1 wt %)–K_2HfF_6 (10 wt %)–NaF (5 wt %) electrolyte with a niobium anode at the cathodic current density 0.12 A cm^{-2} and temperature 1023 K; (a) outer side of the coating; (b) inner side after separation of the coating from the graphite substrate.

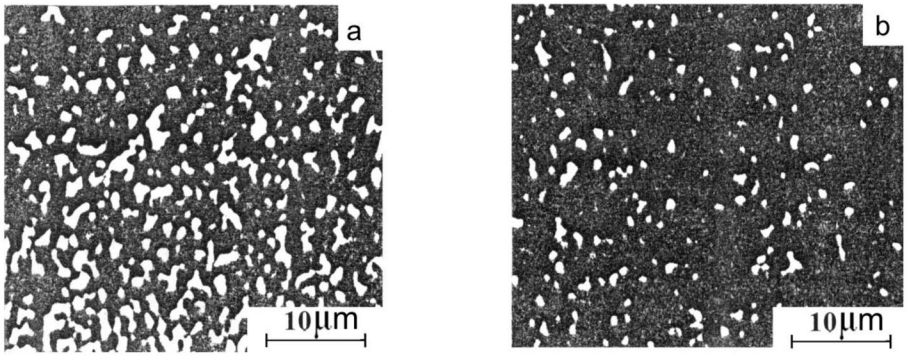

Fig. 7 Scanning images of the Nb–Hf alloys in characterizing rays Nb–L_α; (a) 78.1 wt % Nb; (b) 33.8 wt % Nb.

Reactions of currentless transfer

The phenomenon of currentless transfer or electroless plating of an electronegative metal (Nb) onto a more electropositive substrate from carbon steel (St. 3, St. 45, U8, U10) for deposition of niobium carbide coatings through a molten salt containing niobium compounds was used [44]. An equimolar mixture of NaCl–KCl and a ternary eutectic LiF–NaF–KF (FLINAK) were utilized as background melts. The background NaCl–KCl and LiF–NaF–KF melts were placed in a molybdenum or glassy carbon (SU-2000) container with the walls and bottom lined with the niobium metal. The container was placed in a hermetic retort made of stainless steel (X18N10T) where the operation of evacuating was repeated at room temperature, filled with argon, and then heated to the desired temperature.

A potassium heptafluoroniobate (K_2NbF_7), niobium pentachloride ($NbCl_5$), and high-purity niobium metal were used.

As a reaction medium for the process of niobium currentless transfer onto a carbon steel substrate, the following melts were used:

I NaCl–KCl–$NbCl_5$ (2 wt %)

II NaCl–KCl–K_2NbF_7 (10–30 wt %)

III FLINAK–$NbCl_5$ (10–15 wt %)

IV FLINAK–K_2NbF_7 (10–30 wt %)

On contact of niobium metal with all the above melts a metal–salt reaction, yielding a reduced form of niobium, spontaneously occurs [45]

$$4Nb(V) + Nb \leftrightarrow 5Nb(IV) \quad (13)$$

The Nb(IV) complexes diffuse to the steel substrate and disproportionate on its surface with the formation of niobium carbide [46]

$$5Nb(IV) + C_{(\text{steel surface})} \rightarrow NbC + 4Nb(V) \quad (14)$$

The driving force of reaction 14 is energy of carbide formation ΔG_{NbC}. The Nb(V) complexes appearing in the melt due to reaction 14, diffuse to the niobium metal, enter into reaction with it (reaction 13) with the formation of Nb(IV) complexes. Thus, the process of niobium transfer onto the carbon steel surface is closed in a cycle, and the resulting reaction based on reactions 13 and 14 can be written as

$$Nb + C \rightarrow NbC \quad (15)$$

When employing I–IV melts, in all the cases of carbon steel surfaces, according to XRD analysis, monophase carbide of NbC composition was formed. However, the easiest technological melt is NaCl–KCl–K_2NbF_7 (30 wt %). The drawback of a purely chloride melt (I) is a high vapor pressure resulting in the impossibility of creating a high niobium concentration in the melt, necessary to increase the transfer process intensity. Even at a concentration of 2 wt % $NbCl_5$, the niobium content was observed to diminish in the melt with the course of time. The coatings obtained from the melts on the basis of a ternary eutectic mixture (III–IV) are much harder to wash out of the salts than melts (I–II).

Figure 8 gives an SEM photograph of the substrate surface from the brand St. 3 steel after exposure in NaCl–KCl–K_2NbF_7 melt (10 wt %) during 3 h at the temperature of 1073 K. On the substrate surface, spheroid niobium carbide crystals of the NbC composition can be seen. The intensity of niobium carbide generation in the case of currentless transfer is low, but it enhances with increase of the molten salt temperature and potassium heptafluoroniobate concentration, and using the niobium powder as the metal.

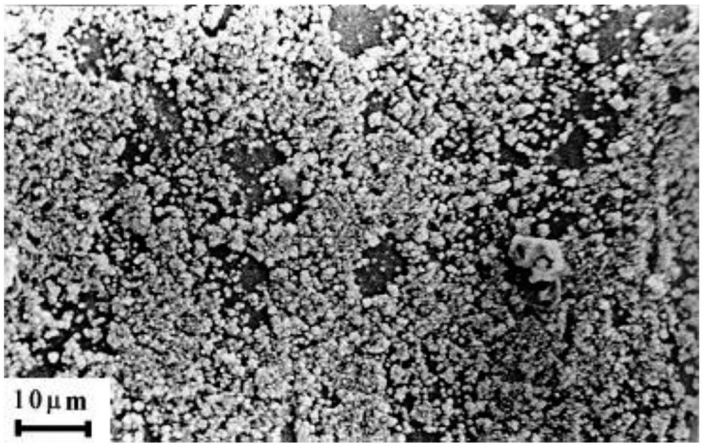

Fig. 8 St. 3 substrate surface morphology after 3 h exposure in NaCl–KCl–K_2NbF_7 (10 wt %) melt in an equilibrium with Nb-metal at 1073 K.

The experiments have shown that at a concentration of 30 wt % K_2NbF_7, using a niobium powder and at 1073 K, in the course of 6 h on the surface of a St. 3 article, a coherent niobium carbide coating 1.5–2 μm thick is produced (Fig. 9). The coating thickness depends on the carbon content in the steel, so for steel of the brand U10 (1.0 wt % C), it is 5–7 μm. The niobium carbide microhardness on high-carbon steels U8 and U10, measured at cross-sections, was 2900–3300 kg mm^{-2}.

Fig. 9 St. 3 substrate surface morphology after 6 h exposure in NaCl–KCl–K_2NbF_7 (30 wt %) melt in an equilibrium with Nb-metal at 1073 K.

Reactions of disproportionation

In the powder metallurgy, the responsible parts are obtained by hot isostatic pressing (HIP). The shape of an article is determined by the shape of the shell used. Shells from ceramics and glassy-ceramics obtained by the method of rejection mask model are the widest spread [47].

Leaking is only one of the drawbacks of the ceramic and glassy-ceramic shells, the most important one being high adhesion and depth of interaction with metals. Interaction of the metal powder with the shell at 1273 K and the pressure of 2000 atm is so vigorous that it is impossible to separate the article from the shell. The reason for the article's intensive interaction with the shell is the chemical processes occurring on the shell–article interface. The thermodynamic calculations performed in the temperature range of 873–1473 K have shown that the titanium alloy components may enter into chemical reactions with oxides incorporated into ceramic and glassy-ceramic shells.

The aforementioned disadvantages can be eliminated by metal deposition onto the shell. The metals to be used as coatings should be sufficiently refractory, i.e., have the melting point not lower than the temperature of the alloy pressing, usually 1273–1473 K.

In this study, for the formation of titanium and niobium barrier layers on glassy-ceramic shells, the reactions of disproportionation (DPP) in molten salts were employed

$$3TiCl_4^{2-} + 2O^{2-} \rightarrow 2TiOCl\downarrow^{-} + Ti + 10Cl^{-} \quad (16)$$

$$5NbF_6^{2-} + 4O^{2-} \rightarrow 4NbOF_6^{3-} + Nb + 6F^{-} \quad (17)$$

The mechanism of DPP reactions was described in detail [14]. It is necessary to note that the DPP reactions with the formation of titanium and niobium coatings are self-controlled as they occur until on the surface remain spots unplated with the metal in the form of a coating. The mechanism of these reactions by itself permits us to obtain uniform, coherent coatings on glassy-ceramic shells of any shape including those having narrow channels, openings.

Pressing of the titanium alloy (PT3V) was carried out in a gasostate at 1273 K, pressure 2000 atm, and the time of compaction 4 h. As a result, articles easily removable from the glassy-ceramic shells were produced.

It was found that the starting metal-glassy-ceramic shells have a coherent layer of the coating on the surface. The titanium layer thickness was 50 μm and that of the niobium-bearing one was 100 μm. During the HIP process, under high temperatures and pressures the coatings become compressed and their thickness diminishes by 25–30 %, but the coherence of the shell's interior surface is not damaged. The microstructure of the PT3V alloy after pressing is presented in Fig. 10. The obtained article sam-

ples have a density close to the theoretical one without any visible structural defects and pores. The character of the microstructure allows us to refer them to the 3–4 type of titanium α-alloys.

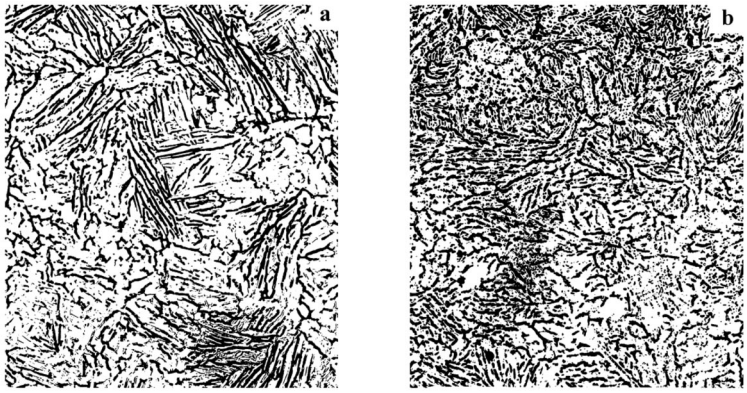

Fig. 10 Microstructure of the titanium alloy after hot isostatic pressing in the glassy-ceramic shells coated with: (a) niobium; (b) titanium.

REFERENCES

1. S. A. Kuznetsov. *Russ. J. Electrochem.* **29**, 1154 (1993).
2. S. A. Kuznetsov. *Russ. J. Electrochem.* **32**, 1209 (1990).
3. S. A. Kuznetsov, S. V. Kuznetsova, P. T. Stangrit. *Rasplavy* **5**, 19 (1991).
4. S. A. Kuznetsov, S. V. Kuznetsova, E. G. Polyakov, P. T. Stangrit. *Rasplavy* **2**, 110 (1988).
5. S. A. Kuznetsov, S. V. Kuznetsova, P. T. Stangrit. *Russ. J. Electrochem.* **28**, 291 (1992).
6. S. A. Kuznetsov, S. V. Kuznetsova, P. T. Stangrit. *Russ. J. Electrochem.* **26**, 63 (1990).
7. S. A. Kuznetsov, S. V. Kuznetsova, P. T. Stangrit. *Russ. J. Electrochem.* **26**, 102 (1990).
8. S. A. Kuznetsov. *Russ. J. Electrochem.* **30**, 1462 (1994).
9. S. A. Kuznetsov, A. G. Morachevskii, P. T. Stangrit. *Russ. J. Electrochem.* **18**, 1522 (1982).
10. S. A. Kuznetsov, A. B. Smirnov, A. N. Shchetkovskii. *Russ. J. Appl. Chem.* **60**, 1730 (1987).
11. S. A. Kuznetsov, A. B. Smirnov, A. N. Shchetkovsky, A. L. Etenko. *Refractory Metals in Molten Salts*, Kluwer Academic, Dordrecht **53/3**, 219 (1998).
12. S. K. D. Strubinger, I.-W. Sun, W. E. Cleland, C. L. Hussey. *Inorg. Chem*. **29**, 4246 (1990).
13. S. A. Kuznetsov. *Molten Salts Forum* **5–6**, 505 (1998).
14. S. A. Kuznetsov, P. T. Stangrit. *Russ. J. Appl. Chem.* **66**, 2702 (1993).
15. S. A. Kuznetsov, S. V. Kuznetsova, V. V. Grinevitch. *Russ. J. Electrochem.* **33**, 259 (1997).
16. G. Kaptay, S. A. Kuznetsov. *Plasmas Ions* **2**, 45 (1999).
17. A. Dent, K. Seddon, T. Welton. *J. Chem. Soc., Chem. Commun*. **4**, 315 (1990).
18. I. V. Zarutskiy, V. V. Malyshev, V. I. Shapoval. *Russ. J. Appl. Chem*. **70**, 1475 (1997).
19. S. A. Kuznetsov, S. V. Devyatkin, A. L. Glagolevskaya. *Rasplavy* **6**, 67 (1992).
20. S. A. Kuznetsov, A. L. Glagolevskaya. *Russ. J. Electrochem.* **32**, 344 (1996).
21. R. S. Nicholson, I. Shain. *Anal. Chem*. **36**, 706 (1964).
22. S. V. Devyatkin, G. Kaptay, V. I. Shapoval, I. V. Zarutskii, V. P. Lugovoi, S. A. Kuznetsov. *Refractory Metals in Molten Salts*, Kluwer Academic, Dordrecht **53/3**, 73 (1998).
23. S. A. Kuznetsov, A. L. Glagolevskaya, A. T. Belyaevskiy. *Russ. J. Appl. Chem.* **67**, 1093 (1994).
24. S. A. Kuznetsov, A. L. Glagolevskaya. *Russ. J. Electrochem.* **31**, 1389 (1995).
25. G. R. Stafford, T. P. Moffat. *J. Electrochem. Soc*. **142**, 3289 (1995).
26. S. A. Kuznetsov. *Russ. J. Electrochem.* **35**, 1301 (1999).
27. A. I. Karasevskii, I. N. Karnaukhov. *J. Electroanal. Chem*. **348**, 49 (1993).

28. F. Lantelme, Y. Berghoute, J. H. von Barner, G. S. Picard. *J. Electrochem. Soc.* **142**, 4097 (1995).
29. F. Matthiesen, E. Christensen, J. H. von Barner, N. J. Bjerrum. *J. Electrochem. Soc.* **143**, 1794 (1996).
30. S. A. Kuznetsov, A. L. Glagolevskaya, V. V. Grinevitch, S. V. Kuznetsova. *Russ. J. Electrochem.* **33**, 234 (1997).
31. B. Gillesberg, N. J. Bjerrum, J. H. von Barner, F. Lantelme. *J. Electrochem. Soc.* **144**, 3435 (1997).
32. U. Stohr, P. R. Bandi, F. Matthiesen, W. Freyland. *Electrochim. Acta* **43**, 569 (1998).
33. F. Matthiesen, P. T. Jensen, T. Ostvold. *Acta Chem. Scand.* **52**, 1000 (1998).
34. V. V. Grinevitch, V. A. Reznichenko, M. S. Model, S. A. Kuznetsov, E. G. Polyakov, P. T. Stangrit. *J. Appl. Electrochem.* **29**, 693 (1999).
35. V. V. Grinevitch, M. S. Model, O. G. Karpinsky, A. V. Arakcheeva, S. A. Kuznetsov, E. G. Polyakov. *Dokl. Chem.* **319**, 389 (1991).
36. V. V. Grinevitch, A. V. Arakcheeva, S. A. Kuznetsov. *J. Min. Metall. B* **39**, 223 (2003).
37. V. D. Shatinskiy, F. I. Nesterenko. *Protecting Diffusional Coatings*, Naukova dumka, Kiev (1988).
38. S. A. Kuznetsov, E. G. Polyakov, S. V. Kuznetsova, P. T. Stangrit. *Russ. J. Appl. Chem.* **61**, 160 (1988).
39. M. A. Tulkina, I. A. Tsuganova. *Russ. J. Inorg. Chem.* **9**, 1650 (1964).
40. Yu. Y. Andreev. *Russ. J. Electrochem.* **15**, 49 (1979).
41. G. I. Ruda, O. Yu. Samgina, V. P. Smirnov. *Prot. Met.* **19**, 984 (1983).
42. A. N. Baraboshkin. *Electrocrystallization of Metals from Molten Salts,* Nauka, Moscow (1976).
43. S. A. Kuznetsov. *Russ. J. Electrochem.* **35**, 1301 (1999).
44. N. G. Ilyushchenko, A. I. Anfinogenov, N. I. Shurov. *Interaction of Metals in Ionic Melts*, Nauka, Moscow (1991).
45. S. A. Kuznetsov, V. V. Grinevitch. *Russ. J. Appl. Chem.* **67**, 1423 (1994).
46. S. A. Kuznetsov. *Russ. J. Appl. Chem.* **72**, 1127 (1999).
47. P. S. Kisly, N. I. Bodnaruk, Ya. O. Gorichok. *Physico-Chemical Foundations of Refractory Superhard Material Production*, Naukova Dumka, Kiev (1986).